Conference paper

Pallavi B. Mungse, Govindachetty Saravanan*, Maiko Nishibori, Jan Subrt and Nitin K. Labhsetwar*

Solvent-free, improved synthesis of pure bixbyite phase of iron and manganese mixed oxides as low-cost, potential oxygen carrier for chemical looping with oxygen uncoupling

DOI 10.1515/pac-2016-1127

Abstract: Chemical looping with oxygen uncoupling (CLOU) is the tendency of releasing gaseous oxygen of an oxygen carrier upon heating, which is the key property for the efficient and cleaner combustion of solid fuels for their wide exploitation for thermal power applications. The solvent-free, improved synthesis method was developed for the synthesis of pure bixbyite, $FeMnO_3$ ($Ia\bar{3}$, $a=b=c=0.94$ nm) as a low-cost, oxygen carrier by exposing of the abundantly available precursors (Fe_3O_4 and MnO) under inert- or reduction- atmosphere followed by air at 900 °C. The bixbyite $FeMnO_3$ showed the enhanced, stable multi-cycle CLOU performance than that of the physical mixture and it is converted into $FeMn_2O_4$ after the complete exhaustion of reactive oxygen under CLOU conditions. $FeMnO_3$ showed the uniform elemental distribution of Fe, Mn and O, which facilitate the regeneration in air upon heating for multi-cycle performance. 3.2 wt.% of reactive oxygen can be obtained compared to the mass of $FeMnO_3$ which is almost equal to the theoretical value under CLOU conditions. The lattice of $FeMnO_3$ is altered linearly above 100 °C with the increase of temperature, however; without the decomposition of the bixbyite phase and it was reinstated virtually upon cooling in air.

Keywords: CO_2 capture and sequestration; lattice; mixed metal oxides; reactive oxygen; SSC-2016; thermal power plants.

Introduction

The considerable use of fossil fuels for energy generation by thermal power plants will continue in the coming years for both developed and developing countries, due to the huge energy demand [1]. Therefore, carbon dioxide (CO_2) as the primary greenhouse gas (GHG), which accounts for one third of the total CO_2 emissions solely from thermal power plants, would emit continuously to the environment due to the combustion of fossil fuels [2–4]. CO_2 capture and sequestration (CCS) is one of the viable among other options to generate

Article note: A collection of invited papers based on presentations at the 12th Conference on Solid State Chemistry (SSC-2016), Prague, Czech Republic, 18–23 September 2016.

***Corresponding authors: Govindachetty Saravanan and Nitin K. Labhsetwar,** CSIR-National Environmental Engineering Research Institute (CSIR-NEERI), Nagpur-440020, India, Tel./Fax: +91-712-2249753, E-mail: g_saravanan@neeri.res.in (G. Saravanan); nk_labhsetwar@neeri.res.in (N. K. Labhsetwar)
Pallavi B. Mungse: CSIR-National Environmental Engineering Research Institute (CSIR-NEERI), Nagpur-440020, India
Maiko Nishibori: Department of Energy and Material Sciences, Faculty of Engineering Sciences, Kyushu University, Kasuga, Fukuoka 816-8580, Japan
Jan Subrt: Institute of Inorganic Chemistry, Academy of Sciences of the Czech Republic, 250 68 Rez., Czech Republic

cleaner energy from fossil fuels, where CO_2 can be captured and stored permanently or it can be used to produce the value added chemicals [5, 6]. The high capital and running cost as well as energy are needed in the existing CCS techniques due to the separation of diluted CO_2 from the exhaust as it contains largely N_2, unreacted O_2, H_2O and other gasses [7]. Chemical looping combustion (CLC) and chemical looping with uncoupling (CLOU) possess the inherent promise of CO_2-separation from the off-gasses than that of existing CCS techniques as they produce virtually CO_2 as the result of enhanced fuel combustion due to the inherent supply of pure gaseous O_2 from the oxygen carrier (e.g. metal oxides, mixed metal oxides, etc.) upon heating [8–10].

The pure phase of mixed metal oxides of Cu and Mn ($CuMn_2O_4$), Fe and Mn ($FeMnO_3$), etc. as low-cost, environmentally benign oxygen carriers are developed recently that can be used as alternative to the currently available oxygen carriers for CLC [11–15]. These mixed oxides form MnO as one of the products after chemical looping combustion reaction using methane, syngas, etc. and it provides the structural stability to their reduced co-products, which facilitates the regeneration of these oxygen carriers upon heating in air (self-supported oxygen carrier) [11–13]. The developed oxygen carrier showed enhanced CLC activity for methane and syngas combustion in terms of multi-cycle performance, stability, CO_2-selectivity, etc. under harsh CLC operational conditions than that of its counterparts (Cu-, Fe- and Mn-oxides) [11–13]. In addition, these oxygen carriers possess CLOU property, which is the tendency of releasing gaseous oxygen from their lattice upon heating [16–18]. In addition to the combustion of gaseous fuels, the CLOU property of oxygen carrier can be exploited for direct combustion of the solid fuels (e.g. coal, biomass, etc.) without prior gasification for thermal power plants applications [17, 19]. The production of pure gaseous oxygen would also find several promising applications in fuel cell-related reactions (e.g. cathodic oxygen reduction reaction), separation of O_2 from air, etc. The cost of these potential oxygen carriers, however, is still high, which restricts the implementation of chemical looping-based technology at a large scale for cleaner energy generation from fossil fuels due to their synthesis methods (e.g. template synthesis, co-precipitation, high energy ball mill, mechanical alloying, etc.), as they require huge amounts of energy, high purity metallic salts, various precipitants, pH control, washing solvents, etc [20–26]. Li et al. reported a facile route for the synthesis of $FeMnO_3$ hollow sphere/reduced graphene oxide composite, where $FeMnO_3$ was synthesized using carbon spheres as sacrificial template and demonstrated its superior electrochemical storage performance for supercapacitor applications [20]. The ferromagnetic $FeMnO_3$ was synthesized through mechano-chemical method using high energy ball milling and its structure was investigated using powder neutron diffraction method [21]. CeO_2-supported $FeMnO_3$ was synthesized through incipient wetness method as oxygen carrier for chemical looping combustion of H_2 and CH_4 [22]. The pure phase of $FeMnO_3$ was synthesized through the oxidative thermal decomposition of $Mn[Fe(CN)_5NO] \cdot 2H_2O$ at 1095 °C [23]. Iron-manganese mixed oxides at nano-order were synthesized through sonochemical method, however, the synthesized bixbyite $FeMnO_3$ nanoparticles showed a small impurity of Mn_2O_3 [24]. The CO oxidation reaction on $FeMnO_3$ and $Pd/FeMnO_3$ catalysts was performed, where these catalysts were prepared through co-precipitation method [25]. The mixed oxides of Fe-Mn were synthesized through co-precipitation methods which were used for low temperature selective catalytic reduction of NO with NH_3 [26]. The authors of this article also demonstrated the stable and multi-cycle CLC performance of the pure phase of $FeMnO_3$ synthesized by co-precipitation method using the nitrate precursors of Fe and Mn and Na_2CO_3 as precipitating agent [12]. Although several methods have been reported for the synthesis of pure bixbyite $FeMnO_3$ either in the form of supported- or unsupported, however, these methods require high synthesis cost due to the use of organic templates, various solvents including washing purpose, high purity Fe and Mn precursors, high energy ball milling, high energy ultrasonicator, precipitating agents etc., which restrict their implementation in chemical looping-based technology at a larger scale for cleaner energy generation from fossil fuels. The expenditure for the synthesis of these oxygen carriers can be reduced significantly for the wide exploitation of chemical looping-based technology by the selection of low-cost synthesis method, abundantly available minerals, ores, etc.

Here, we successfully developed a solvent-free, improved synthesis method to prepare the pure bixbyite $FeMnO_3$ phase as potential oxygen carrier without using any solvent, precipitants and any sophisticated technique or process. $FeMnO_3$ was successfully synthesized by sequentially exposing of the stoichiometric

precursors (3:1) of MnO and Fe_3O_4 under N_2 or reducing conditions (H_2 or CH_4) followed by air at 900 °C, which showed a stable and enhanced multi-cycle, CLOU performance (10 cycles) (Scheme 1). These oxides were selected as the precursors for the synthesis due to the formation of Fe_3O_4 and MnO as thermodynamically stable products after CLC reaction of $FeMnO_3$ for CH_4 combustion [12].

Experimental

Materials

The oxide precursors of Fe and Mn used for the synthesis of Fe-Mn mixed oxide (bixbyite, $FeMnO_3$) were of analytical grade and used without further purification. Iron (II, III) oxide, Fe_3O_4 (98 %) and Manganese (II) oxide, MnO (99.99 %) used for the synthesis were purchased from Sigma Aldrich.

Synthesis of $FeMnO_3$

The pure bixbyite $FeMnO_3$ phase was synthesized by the solvent-free, improved synthesis method by sequentially exposing of the stoichiometric precursors (3:1) of MnO and Fe_3O_4 under N_2 or reducing conditions (H_2 or CH_4) followed by air at 900 °C. The manganese (II) oxide, MnO (4.25 g) and Iron (II, III) oxide, Fe_3O_4 (4.63 g) were mixed thoroughly for 2 h using mortar and pestle. The resultant physical mixture was then converted into small pellets of uniform size of 1 mm using the pelletizer followed by sieving (mesh size = 1 mm) to avoid any back pressure due to the fine nature of powder sample during the evaluation. One gram of pellets was sandwiched between quartz wool inside the quartz reactor, which was placed inside the temperature controlled tubular furnace (Applied test systems, Inc.). The pellets were subjected to heat treatment either under inert (N_2) atmosphere or under H_2 (5 %) or CH_4 (5 %) balanced with Helium at 900 °C for 5 h. The reduced sample was then subjected to aerial oxidation at 900 °C in air for 12 h to form the pure phase of bixbyite $FeMnO_3$. The physical mixture of Fe_3O_4 and MnO, is used as an internal reference to $FeMnO_3$ synthesized through solvent-free, improved synthesis method.

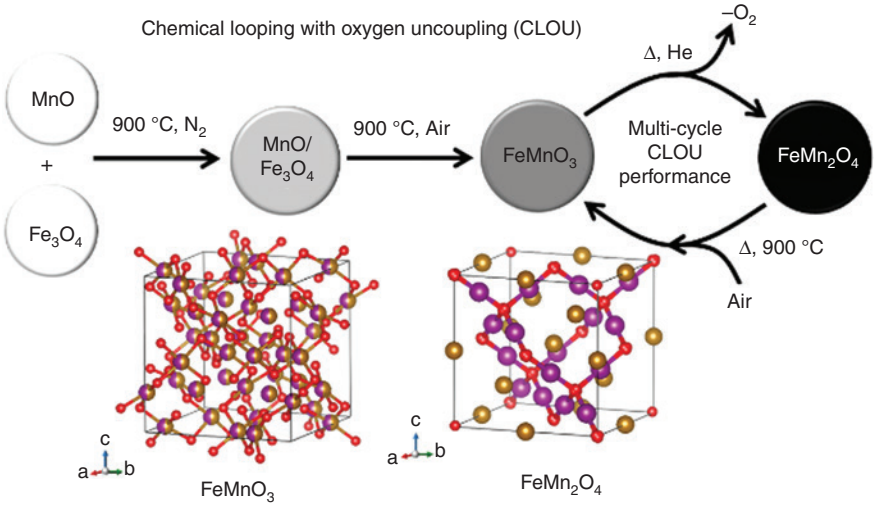

Scheme 1: Schematic illustration of solvent-free, improved synthesis of bixbyite, $FeMnO_3$ phase and its multi-cycle chemical looping with oxygen uncoupling performance. Ball and stick models show the crystal structures of $(Fe, Mn)_2O_3$ and $(Fe, Mn)_3O_4$. Brown, purple and red balls correspond to Fe, Mn, and O, respectively.

Characterization

The formation of pure bixbyite $FeMnO_3$ phase and physical mixture of Fe_3O_4 and MnO as the internal reference counterpart were structurally identified using an X-ray diffractometer (Rigaku: Miniflex-II-DD34863) operated at 30 kV and 15 mA with a monochromatized CuKα radiation (λ = 0.15418 nm) in 2θ range between 20 and 90° and at a scan rate of 1° min^{-1}. The formation of bixbyite phase was identified using ICDD (international center for diffraction data) database. The surface morphology of Fe-Mn mixed oxides was investigated using a SEM instrument (Nova NanoSEM 450) operated at an accelerating voltage of 18–30 kV. Elemental dispersion of the synthesized products was examined using energy dispersive spectroscopy (EDAX GENESIS) at a mapping time of 6 μs. Temperature controlled *p*XRD analysis of $FeMnO_3$ was carried out using the X-ray diffractometer (Rigaku: Ultima IV) using the Cu Kα radiation operated at 30 kV and 40 mA to study the lattice strains. Thermogravimetric analysis (TGA) of the bixbyite $FeMnO_3$ was performed using a TGA instrument (TG 6300 SII Nano Technology Incorporation, Japan). $FeMnO_3$ was heated from room temperature to 1010 °C at a ramping rate of 10 °C min^{-1} under N_2 flow of 100 mL min^{-1} followed by cooling under the same condition.

Evaluation of CLOU performance

CLOU performance of bixbyite $FeMnO_3$ and its reference counterpart was evaluated by a temperature programmed desorption (TPD) method using a Micromeritics instrument (Autochem-II 2920) equipped with a thermal conductivity detector (TCD). 0.1 g of the sample was sandwiched between quartz wool inside a U-shaped quartz reactor, which was placed inside the temperature controlled furnace. For O_2-TPD analysis, the sample was preheated at 200 °C (ramp rate 5° min^{-1}) in the presence of air at a flow rate of 15 mL min^{-1} for 30 min to saturate the O_2 vacancies of the sample, if any, followed by cooling down to 50 °C in the same air flow. The temperature of the sample then increased up to 1000 °C in the presence of helium at a flow rate of 10 mL min^{-1} and desorbed O_2 was analyzed using the TCD detector. In order to investigate the multicycle CLOU performance, the sample was re-oxidized after each TPD cycle by temperature programmed oxidation (TPO) method using the same instrument, wherein the sample was heated at 900 °C in the presence of air at a flow rate of 50 mL min^{-1} for 5 h. The re-oxidized sample was again subjected to a second cycle of TPD. In this way multiple TPD-TPO cycles were performed to evaluate the multi-cycle CLOU performance of $FeMnO_3$.

Results and discussion

Figure 1a shows the *p*XRD profile of the products synthesized through the solvent-free, improved synthesis method. The products showed the characteristic diffraction peaks at 23.1°, 32.9°, 38.3°, 45.2°, 49.3°, 55.2° and 65.8° for the reflection planes of (211), (222), (400), (332), (431), (440) and (622), respectively, correspond

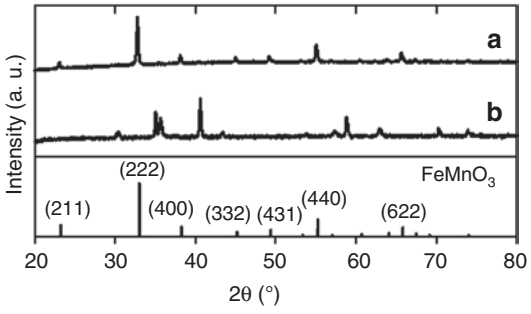

Fig. 1: *p*XRD profiles of $FeMnO_3$ prepared through solvent-free, improved synthesis method (a) and the physical mixture of MnO and Fe_3O_4 (b). The simulated XRD lines for $FeMnO_3$ are shown for reference purpose.

to the pure bixbyite $FeMnO_3$ phase ($Ia\bar{3}$, $a=b=c=0.94$ nm) (hereafter denoted as FMO). The *p*XRD profile for the physical mixture shows the characteristic diffraction peaks at 29.5°, 34.8°, 42.3°, 52.4°, 55.8°, 61.4° and 61.5° for the reflection planes of (112), (103), (220), (312), (321), (224) and (400) respectively, correspond to Fe_3O_4 (*Imma*; $a=b=0.59$ nm, $c=0.83$ nm) along with the characteristic diffraction peaks at 34.8°, 40.4°, 58.7°, 69.7° and 87.7° for the reflection planes of (111), (200), (220), (311) and (400) respectively, correspond to MnO ($Fm\bar{3}m$; $a=b=c=0.44$ nm) (Fig. 1b). It should be noted that the pure bixbyite phase of FMO without any impurities was obtained when the precursors were subjected also under H_2 or CH_4 followed under air at 900 °C (see Supporting Information, Fig. S1). These results suggest that the pure bixbyite phase can be synthesized by treating the abundantly available precursors under reduction followed by oxidation conditions.

The precursors treated under N_2, H_2 and CH_4 (i.e. reductions conditions) at 900 °C were analysed by *p*XRD to examine the influence of reduction conditions to the precursors. Figure 2 shows the *p*XRD profile of the physical mixture of MnO and Fe_3O_4 after the reduction treatment under N_2, H_2 and CH_4 atmosphere. No significant difference, however, the characteristic diffraction peaks of Fe_3O_4 and MnO are slightly shifted to the lower diffraction angle when the precursors were treated under N_2 atmosphere at 900 °C (Fig. 2b). The precursors treated under CH_4 atmosphere showed the characteristic diffraction peaks at 29.6°, 34.9°, 42.4°, 56° and 61.5° for the reflection planes of (220), (311), (400), (333) and (440), respectively, correspond to $Mn_{1.03}Fe_{1.97}O_4$ ($Fd\bar{3}\,m$; $a=b=c=0.85$ nm) along with the characteristic diffraction peaks of MnO (Fig. 2c). Whereas, the precursors treated under H_2 atmosphere showed the characteristic diffraction peaks at 35.4°, 41.1°, 59.6°, 71.3°, 75° and 89.3° for the reflection planes of (111), (200), (220), (311), (222) and (400), respectively, correspond to $(FeO)_{0.497}(MnO)_{0.503}$($Fm\bar{3}m$; $a=b=c=0.43$ nm) (Fig. 2d). These results imply that the precursors are uniformly mixed through solid-state reaction under reduction conditions at elevated temperature. This would most likely facilitate the formation of pure mixed oxide form upon heating in air at elevated temperature through exothermic reaction which was further rationalized by performing the FE-SEM and elemental mapping of the precursors of Fe_3O_4 and MnO after the reduction treatment at 900 °C (see Figs. 3 and 4 for the details).

Figure 3a shows the FE-SEM image of the physical mixture of Fe_3O_4 and MnO. The precursors were thoroughly mixed for 2 h and performed the microscopic observation of the resultant products. It shows the large-sized, agglomerated particles with irregular shapes and sizes. It also shows the non-uniform Fe and Mn distributions throughout the products as shown in Fig. 3b–c.

Figure 4a shows the FE-SEM image of the physical mixture of Fe_3O_4 and MnO after reduction treatment at 900 °C. The large-sized, agglomerated particles with random in shapes and sizes were again observed after the reduction treatment. Whereas, the elemental mapping images (Fig. 4b–d) show the uniform distribution of Fe, Mn and O throughout the surface which most likely facilitates the formation of pure bixbyite phase on aerial oxidation at 900 °C. The physical mixture of Fe and Mn-precursors undergoes solid-state reaction when they expose under reduction conditions that induce the formation of mixed oxides. The composition of

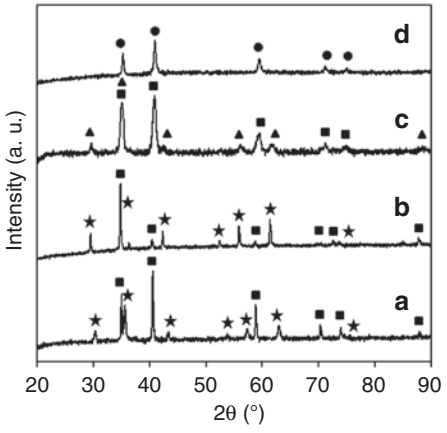

Fig. 2: *p*XRD profiles of the physical mixture of MnO and Fe_3O_4 (a) after subjecting under N_2 (b) CH_4 (c) and H_2 (d). MnO (■), Fe_3O_4(★), $Mn_{1.03}Fe_{1.97}O_4$(▲), $(FeO)_{0.497}(MnO)_{0.503}$(●).

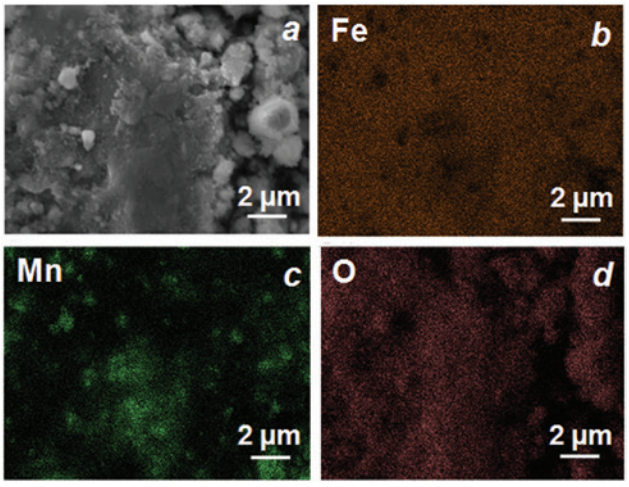

Fig. 3: FE-SEM image of the physical mixture of Fe_3O_4 and MnO (a) and its elemental mapping of Fe, Mn, and O (b–d).

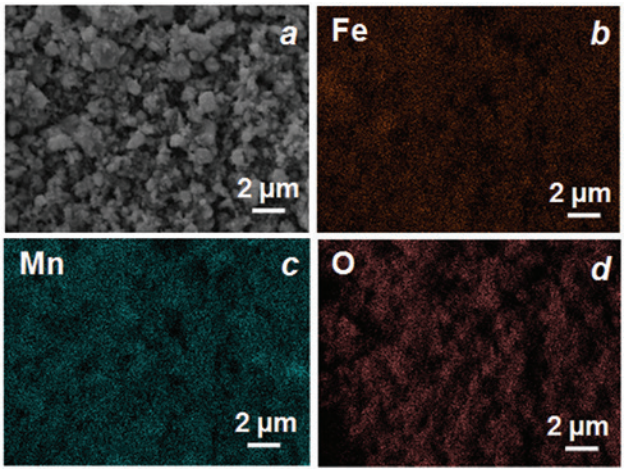

Fig. 4: FE-SEM image of the physical mixture of Fe_3O_4 and MnO after reduction treatment at 900 °C (a) and its elemental mapping of Fe, Mn, and O (b–d).

mixed oxides under different reduction conditions is strongly dependent on the reduction potential of reducing agents. Despite the significant difference in the composition of mixed oxides after reduction treatment using various reducing agents, the pure bixbyite $FeMnO_3$ phase was observed when they treat under air at 900 °C. These results suggest that the formation of mixed oxide phase of the precursors is the key to realize the pure mixed oxide of bixbyite $FeMnO_3$ phase. It should be noted that the direct calcination of the physical mixture of Fe and Mn-precursors in air at 900 °C was not resulted the pure bixbyite $FeMnO_3$ phase and it forms always with some impurities. Therefore, the pure bixbyite $FeMnO_3$ phase can be prepared easily through the solvent-free, improved synthesis method without using any solvents, precipitants, sophisticated techniques, etc, under reduction followed by oxidation conditions.

The large-sized, agglomerated bixbyite FMO clusters with random in shapes and sizes were observed as shown in Fig. 5a. The FMO particles were agglomerated to form the large-sized clusters due to the harsh synthesis conditions (Fig. 5b). It should be noted that the morphology of oxygen carriers is not influenced significantly for both CLC and/or CLOU performance in the case of mixed oxides of Fe-Mn and Cu-Mn. In fact, we reported previously that the significant difference in morphology was observed both in the fresh-and CLC-treated oxygen carrier, however, their oxygen carrying capacity was not at all compromised with the increase of CLC cycles [11, 12]. The observed stable, enhanced multi-cycle CLC performance of the oxygen carrier is

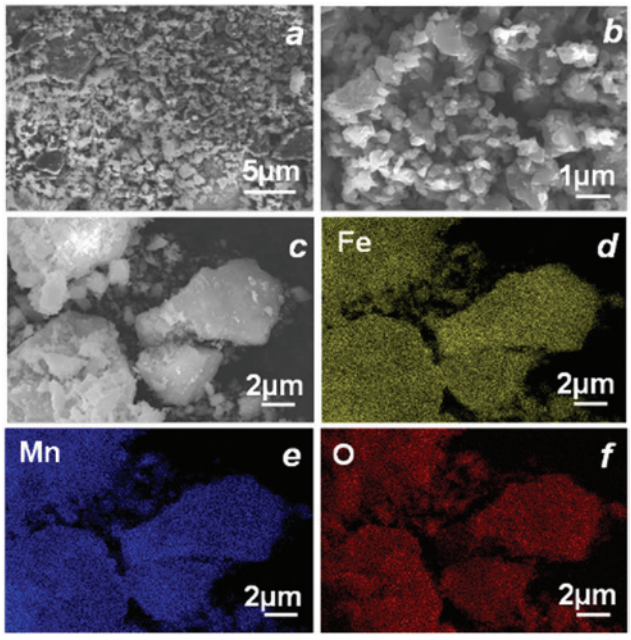

Fig. 5: FE-SEM image of bixbyite $FeMnO_3$ (a) and its magnified image (b). Elemental mapping of Fe, Mn and O (d–f) of the randomly selected agglomerate of bixbyite $FeMnO_3$ (c).

rationalized to the uniform distribution of their counter oxides of MnO and Fe_3O_4 as the final reduced products [11, 12]. Therefore, elemental mapping of FMO was performed on the randomly selected agglomerate to examine the elemental distribution of Fe, Mn, and O as shown in the FE-SEM image (Fig. 5c). As expected, Fe, Mn and O of FMO are uniformly distributed throughout the agglomerates as shown in Fig. 5d–f, which likely facilitate the regeneration in air upon heating for multi-cycle performance. However, the elemental mapping of Fe, Mn, and O of physical mixture of Fe_3O_4 and MnO showed that they are not uniformly distributed in the agglomerates (Fig. 3) which likely affect the CLC and CLOU performance (see Fig. 6b for the details).

The CLOU performance (i.e. O_2-releasing behavior upon heating) of FMO and physical mixture of MnO and Fe_3O_4 for the reference purpose was examined in the presence of helium by the TPD method. The oxygen carrier that releases gaseous oxygen at higher temperature (750–1000 °C) is usually preferred owing to the advantages of heat transfer for power production in the thermal power plants [27, 28]. FMO showed a strong,

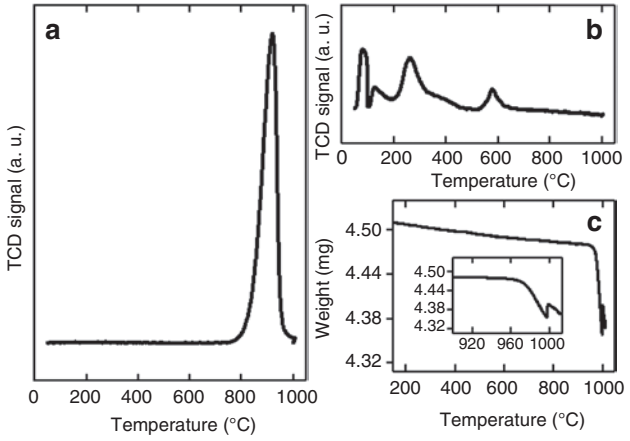

Fig. 6: Temperature programmed oxygen desorption profile of bixbyite $FeMnO_3$ prepared through solvent-free, improved synthesis method (a), the physical mixture of Fe_3O_4 and MnO (b), Thermogravimetric analysis of bixbyite $FeMnO_3$ (c).

single O_2 desorption peak at 920 °C without showing any O_2 desorption at lower temperatures as shown in Fig. 6a. The physical mixture of MnO and Fe_3O_4 (Fig. 6b) also showed the O_2 desorption peaks, however, at relatively weaker O_2 desorption and at a lower temperature range (Fig. 6b) compared to that of FMO, which is usually not favorable for oxygen carrier for thermal power plants applications. The amount of desorbed O_2 upon heating was estimated for both FMO and the physical mixture of MnO and Fe_3O_4. The estimated amount of the desorbed O_2 from FMO is to be 0.99 mmoles g^{-1}, which is significantly higher than that of its stoichiometric physical mixture of Fe_3O_4 and MnO (0.19 mmoles g^{-1}). These results clearly infer that the physical mixture of the individual oxides as oxygen carrier possesses inferior performance and may not be suitable for long-term CLC or CLOU applications. The estimated desorbed O_2 amount of FMO is 3.2 wt.% compared to the mass of FMO, which is almost same to its theoretical O_2 desorption amount of FMO under CLOU conditions ($3(Fe, Mn)_2O_3 \rightarrow 2(Fe, Mn)_3O_4 + 1/2O_2$) [15]. TGA of FMO was performed further to examine the weight loss due to the desorption of oxygen through CLOU. FMO showed the sharp weight loss of 0.15 mg between 150 and 1010 °C, which is again equal to 3.3 wt.% to the mass of FMO (Fig. 6c). Both TPD and TGA results are in excellent agreement with the theoretical O_2 desorbed amount of FMO under CLOU conditions. The reduced oxygen carrier after CLOU performance by TPD and TGA methods was analysed further to identify the product after desorption of gaseous O_2, which shows the spinel phase of $FeMn_2O_4$ ($Fd\bar{3}m$, $a = b = c = 0.85$ nm) (see Supporting Information, Fig. S2). A minor phase of Fe_2O_3 was obtained due to the decomposition of $FeMn_2O_4$ at higher temperature above 1000 °C in the case of the reduced oxygen carrier by the TGA analysis as shown in the inset of Fig. 6c (see Supporting Information, Fig. S3).

Temperature programmed *p*XRD analysis of FMO was performed to examine the structural changes in particular lattice due to the release of oxygen upon heating from room temperature to 950 °C (Fig. 7a). It should be noted that the oxide materials induce lattice strains at higher temperatures [29, 30]. FMO was heated gradually at set temperatures in N_2-environment and cooled down to room temperature in air. FMO showed the characteristic diffraction peak at 32.9° for the reflection plane of (222), which showed no significant changes up to 100 °C, however, it showed the linear shift towards lower diffraction angle upon heating up to 950 °C. Interestingly, the characteristic diffraction peak was virtually retained back to its original peak position upon cooling down to room temperature in air. The lattice constant of FMO ($a = 0.940$ nm at 50 °C) showed the linear increment after 100 °C with the increase of temperature and reached to 0.9474 nm at 950 °C. It was, however, retained virtually back to the original lattice value upon cooling in air to room temperature (Fig. 7b). These results infer that the lattice of FMO was altered significantly upon heating and cooling in N_2-environment and air, respectively. FMO is not released the oxygen when it is heated up to 100 °C, however, it starts releasing the oxygen from their lattice which creates vacant sites in its lattice that induces the relaxation in the lattice structure of FMO. Hence, the characteristic diffraction peaks of FMO are shifted to lower diffraction angles upon heating above 100 °C. When the reduced FMO is cooled down in air from 950 °C to room temperature, the oxygen vacant sites are re-filled again by the oxygen derived from air to its original sites and thus the characteristic diffraction peaks of FMO are re-appeared again. The lattice constant also retained back upon cooling down in air from 950 °C to room temperature.

The stable and multi-cycle performance of oxygen carrier is essentially required to realize them as potential oxygen carrier. The oxygen carrier was re-oxidized after the CLOU reaction (i.e. complete exhaustion of removable O_2 from oxygen carrier) after each successive cycle to examine its multi-cycle CLOU performance. Spinel $FeMn_2O_4$ as the reduced product of oxygen carrier was re-oxidized in air at 900 °C for 5 h and the product was characterized by *p*XRD. As expected, the bixbyite phase of FMO was regenerated upon re-oxidation (see Supporting Information, Fig. S4). The regenerated oxygen carrier was examined for its multi-cycle CLOU performance. Figure 8 shows the TPD profiles of FMO for 10 cycles, which showed no significant difference in the TPD profiles. FMO showed the strong O_2 desorption peak at 920 °C and showed no change at all in O_2 desorption temperature. It is noteworthy to mention that the bixbyite $FeMnO_3$ phase was retained without forming any impurities even after 10 CLOU cycles. The amount of desorbed O_2 in the case of FMO was quantified by integration of the desorption peak and presented in the inset of Fig. 8. The amount of desorbed O_2 for the first cycle was estimated to be 0.99 mmoles g^{-1} which was not changed significantly with the increase of cycles. These results imply that the solvent-free, improved synthesis method developed in this work can be

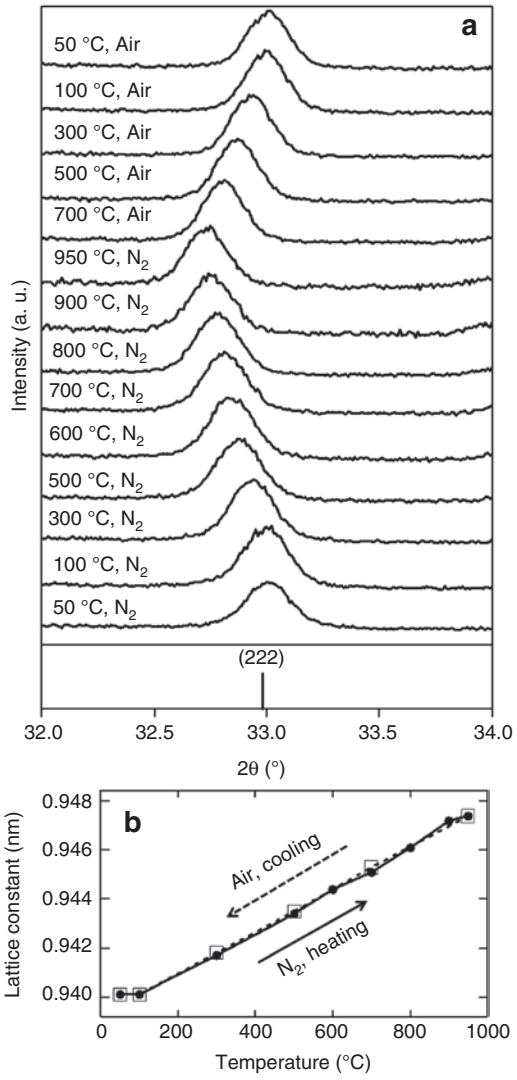

Fig. 7: Temperature programmed *p*XRD profiles of $FeMnO_3$ at set temperatures in N_2 and air (a). The temperature dependence of lattice constant of $FeMnO_3$ (b). $FeMnO_3$ was heated in N_2 (closed circle) up to 950 °C and cooled down to 25 °C in air (open square).

employed for the large scale synthesis of bixbyite $FeMnO_3$ which possesses the potential as oxygen carrier for the CLOU application compared to the individual oxides.

Conclusion

The simple solvent-free, improved synthesis method was developed to prepare the pure bixbyite $FeMnO_3$ phase as low-cost, potential oxygen carrier without using any solvents, precipitants and/or any other sophisticated techniques. The abundantly available precursors of Fe_3O_4 and MnO with 1:3 stoichiometry were mixed uniformly and calcined in the presence of N_2 or reduction conditions (H_2 or CH_4) followed by air at 900 °C to yield the pure bixbyite $FeMnO_3$ phase. The large-sized, agglomerated clusters of $FeMnO_3$ showed the uniform elemental distribution of Fe, Mn and O which facilitate its excellent regeneration upon heating in air for multicycle performance. $FeMnO_3$ released the lattice O_2 upon heating through CLOU mechanism which was confirmed by O_2-TPD and TGA. The desorbed oxygen amount (3.2 wt.% compared to the mass of $FeMnO_3$) is

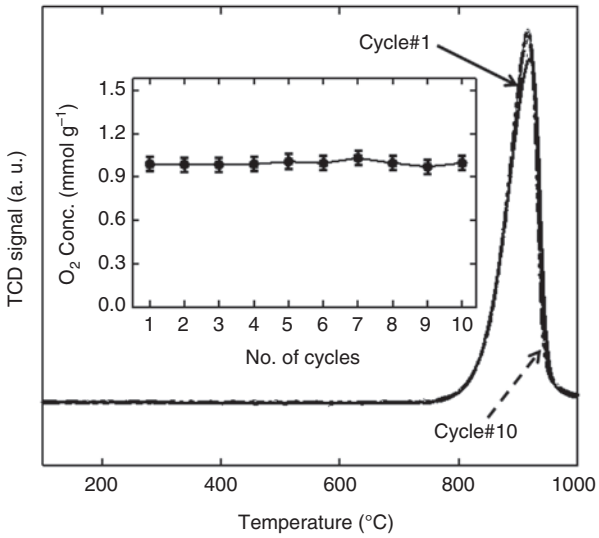

Fig. 8: Cyclic performance of temperature programmed oxygen desorption (TPD) profiles of bixbyite $FeMnO_3$ prepared through solvent-free, improved synthesis method. Inset shows the dependence of oxygen concentration as a function of cycles.

almost equal to the theoretical O_2 desorption amount of $FeMnO_3$ under CLOU conditions. The lattice constant of $FeMnO_3$ increased linearly with the increase of temperature, however, without decomposition of bixbyite structure at 900 °C and it is virtually retained back to its original structure upon cooling in air at 900 °C. $FeMnO_3$ showed enhanced, multi-cycle CLOU performance than that of the physical mixture of its precursors MnO and Fe_3O_4. The spinel phase, $FeMn_2O_4$ was formed as the reduced product after CLOU reaction and can be readily regenerated to bixbyite $FeMnO_3$ upon heating in air at 900 °C. The developed solvent-free, improved method for the synthesis of mixed oxides in pure form would find not only in CCS- but also in catalysis-related applications.

Acknowledgments: The authors thank Council of Scientific and Industrial Research (CSIR), Govt. of India (TapCoal, project No. CSC0102) for financial support. Ms. P. Mungse acknowledge CSIR, India for providing Senior Research Fellowship. Part of these studies have been carried out under the Indo-Czech research collaboration between CSIR-NEERI and IIC Rez. The authors thank Prof. Sonawane, VNIT, Nagpur for the TG analysis. The authors also thank CSIR-National Chemical Laboratory, Pune for FE-SEM studies. KRC No.: 2016\JUN\EMD\5.

References

[1] World Energy Outlook 2015; International Energy Agency: Paris, France (2015).
[2] H. Houghton. *Global Warming: The Complete Briefing*, 3rd ed., Cambridge University Press, New York (2004).
[3] A. Lyngfelt, B. Leckner, T. Mattisson. *Chem. Eng. Sci.* **56**, 3101 (2001).
[4] M. Johansson, T. Mattisson, A. Lyngfelt. *Energ. Fuel* **20**, 2399 (2006).
[5] E. A. Quadrelli, G. Centi, J. L. Duplan, S. Perathoner. *ChemSusChem* **4**, 1194 (2011).
[6] Advancing Clean Electric Power Technologies. Carbon dioxide capture and storage value added options, Chapter 4, Quadrennial Technology Review (2015).
[7] J. Adanez, A. Abad, F. Garcia-Labiano, P. Gayan, L.F. De Diego. *Prog. Energ. Combust. Sci.* **38**, 215 (2012).
[8] M. M. Hossain, H. I. De Lasa. *Chem. Eng. Sci.* **63**, 4433 (2008).
[9] H. Fang, L. Haibin, Z. Zengli. *Int. J. Chem. Eng.* **2009**, 1 (2009).
[10] A. Nandy, C. Loha, S. Gu, P. Sarkar, M. Karmakar, P. Chatterjee. *Renew. Sust. Energ. Rev.* **59**, 597 (2016).
[11] P. Mungse, G. Saravanan, T. Uchiyama, M. Nishibori, Y. Teraoka, S. Rayalu, N. Labhsetwar. *Phys. Chem. Chem. Phys.* **16**, 19634 (2014).

[12] P. Mungse, G. Saravanan, S. Rayalu, N. Labhsetwar. *Energ. Technol.* **3**, 856 (2015).
[13] S. Sajen, S. K. Singh, P. Mungse, S. Rayalu, K. Watanabe, G. Saravanan, N. Labhasetwar. *Energ. Fuels* **30**, 7596 (2016).
[14] A. M. Azad, A. Hedayati, M. Ryden, H. Leion, T. Mattisson. *Energ. Technol.* **1**, 59 (2013).
[15] G. Azimi, M. Ryden, H. Leion, T. Mattisson, A. Lyngfelt. *AIChE J.* **59**, 582 (2013).
[16] Q. Imtiaz, D. Hosseini, C. Rudiger. *Energ. Technol.* **1**, 633 (2013).
[17] A. Lyngfelt. *Appl. Energ.* **113**, 1869 (2014).
[18] M. Ryden, H. Leion, T. Mattisson, A. Lyngfelt. *Appl. Energ.* **113**, 1924 (2014).
[19] H. Leion, T. Mattisson A. Lyngfelt. *Energy Procedia* **1**, 447 (2009).
[20] M. Li, W. Xu, W. Wang, Y. Liu, B. Cui, X. Guo. *J. Power Sources* **248**, 465 (2014).
[21] S. Rayaprol, S. D. Kaushik, P. D. Babu, V. Siruguri. *AIP Conference proceedings* **1132**, 1132 (2013).
[22] S. Bhavsar, B. Tackett, G. Veser. *Fuel* **136**, 268 (2014).
[23] D. Lick, D. B. Soria. *J. Argent. Chem. Soc.* **97**, 102 (2009).
[24] J. I. Lai, K. V. P. M. Shafi, A. Ulman, N. L. Yang, M. H. Cui, T. Vogt, C. Estournes. *Prepr. Pap.-Am. Chem. Soc., Div. Fuel Chem.* **48**, 730 (2003).
[25] S. K. Kulshreshtha, S. Sharma, R. Vijayalakshmi, R. Sasikala. *Indian J. Chem. Technol.* **11**, 427 (2004).
[26] R. Q. Long, T. Yang, R. Chang. *ChemComm* **5**, 452 (2002).
[27] M. Ishida, H. Jin. *Energy* **19**, 415 (1994).
[28] M. Ishida, H. Jin. *Ind. Eng. Chem. Res.* **35**, 2469 (1996).
[29] G. K. Bichile, R. G. Kulkarni. *J. Phys C Solid State Phys.* **8**, 3988 (1975).
[30] A. J. Saldivar-Garcia, H. F. Lopez. *Metall. Mater. Trans. A* **35A**, 2517 (2004).

Supplemental Material: The online version of this article (DOI: 10.1515/pac-2016-1127) offers supplementary material, available to authorized users.